JOURNAL OF MATERIALS SCIENCE 31 (1996) 4311–4319

# Coarsening kinetics of γ′ precipitates in Ni–Al and Ni–Al–Mo alloys

Y. Y. QIU
*Departamento de Engenharia de Materiais, Instituto Superior Técnico, Avenida Rovisco Pais, 1096 Lisboa, Portugal*

The ordered $L1_2$ γ′ precipitate coarsening kinetics without the influence of an external stress were studied in a Ni–Al(13.5 at%) alloy at 1413 K and a Ni–Al(13.8 at%)–Mo(5.9 at%) alloy at 1443 K. The Ni–Al–Mo alloy has a lattice mismatch of about −0.3% at the ageing temperature while the Ni–Al has a positive lattice mismatch of about 0.25% at the ageing temperature. For both alloys, the precipitates were initially cuboidal. After ageing for 3–10 min, the precipitates in the Ni–Al–Mo alloy split mostly into two parallel plates (doublets) or eight sub-cubes (octets), but the initial cuboidal precipitates in the Ni–Al alloy only showed the tendency to split into doublets. After further ageing, the precipitates in both alloys eventually aligned and agglomerated into groups consisting of many particles separated by a small distance of ~30 nm, and the distribution of the precipitates became inhomogeneous. There was no linear relationship between the cube of the average precipitate size and the ageing time as predicted by the classical Lifshitz–Slyozov–Wagner theory. Instead, a retardation of the coarsening process is found.

## 1. Introduction

It is known that the elastic stress generated by a precipitate/matrix mismatch strongly influences the development of both the precipitate morphology and the interparticle spatial correlation during the coarsening in coherent solids. In the Ni–Al system, for example, when the particles are small and the interfacial-to-elastic energy ratio is large, the particles are spherical and nearly randomly distributed. However, as they coarsen, the ratio of the interfacial energy to the elastic energy decreases and the morphology of the particles changes from a spherical to a cuboidal shape. This results in the particles becoming aligned in strings along elastically soft crystallographic directions of the matrix or forming nearly periodic arrays [1–4]. Examples of the effects of elastic stress on the morphological development of particles have been observed by many authors [1–11]. Some of them [3, 5, 8] found that in Ni–Al, after certain times of ageing at high temperature, the γ′ precipitates will spontaneously split, eventually forming eight smaller particles in place of one large particle. The same phenomenon has also been observed in the Ni–Al–Mo system [11]. On the other hand, a growth law $R \propto t^m$ with $m < 1/3$ has been reported [6, 9–11].

The coarsening behaviour in a system where the elastic stress is less important can be theoretically described by the models of Lifshitz and Slyozov, and also Wagner (LSW) [12–13] as well as by modified LSW theories such as the BW [14], LSEM [15] and TK [16] models. The LSW theory assumes that the volume fraction of the precipitate is negligible. The modified LSW theories [14–16] take the effect of the volume fraction of the precipitates into account. All of these theories predict a power law dependence of the average particle radius $R$ on time $t^{1/3}$ and this time dependence has been confirmed in many experiments. The particle size distributions (PSDs) predicted by these theories are independent of ageing time. Both LSW and modified LSW theories however fail to explain the coarsening phenomenon in coherent solids since they neglect the effect of the elastic stress. Several theories considering the effect of an elastic stress field have therefore been developed to predict the coarsening behaviour in such system [17–19].

However, the coarsening kinetics in elastically constrained systems are still controversial and still no theory can explain the experimental observations. More systematic experimental work on for example the growth laws and the size distributions, are required. This paper reports on the influence of the magnitude and sign of the lattice mismatch on the ordered $L1_2$ γ′ precipitate coarsening behaviour. Ni–Al and Ni–Al–Mo systems are used for this study. The Al content was adjusted to maintain the volume fraction of the precipitates and the Mo was added to achieve different lattice mismatches. The composition of both alloys were closely controlled to obtain only two phases; which are the ordered γ′ and the disordered, Ni-rich, f c c γ phases. The magnitude and the sign of the γ′/γ lattice mismatch δ is defined as the relative difference of the two lattice parameters $a_{\gamma'}$ and $a_\gamma$ of the γ′ precipitates and the matrix, respectively, $\delta = (a_{\gamma'} - a_\gamma)/a_\gamma$. Convergent-beam electron diffraction (CBED) was used to measure the γ′/γ lattice mismatch. The CBED patterns are two-dimensional

0022–2461 

maps of diffraction intensity as a function of the inclination between the incident electrons and a particular crystal direction. They are normally composed of a series of discs each one corresponding to a different Bragg reflection. The higher-order Laue zone (HOLZ) lines (in which we are interested) are formed in the central bright-field disc of a CBED pattern by diffraction of incident electrons into reflections in the upper layers of the reciprocal lattice. Because of the large reciprocal lattice vectors involved, the position of HOLZ lines are extremely sensitive both to the operating voltage of the microscope and to the lattice parameters. The accurate measurements of the lattice parameters can be made with respect to a known standard with the same crystal structure. Usually, Si is used as such a standard. The HOLZ lines can be observed by using a condenser (C2) lens system to control the spot size and to focus the electron probe onto the specimen surface to obtain the CBED patterns. The CBED method has been used to study the spatial variation of $\delta$ for several undeformed superalloys [20, 21] and to determine the relative values of strains and lattice mismatch [22]. The measurements of the lattice parameters by the CBED method are based on the comparison of simulated HOLZ patterns in the kinematics approximation with experimental patterns [21, 23, 24].

## 2. Experimental procedure

Cylindrical single crystals Ni–Al and Ni–Al–Mo (5 mm in diameter) with the axis along $\langle 100 \rangle$ were grown by the electron-beam zone melting technique. Disc-shaped specimens (2 mm thick, with $\{100\}$ faces) were cut from crystals that were homogenized at 1573 K for 100 h. The compositions of the disc specimens were checked by electron microprobe analysis. Specimens with compositions of Ni–13.5 at % Al (alloy A) and Ni–13.8 at % Al–5.9 at % Mo (alloy B) were used for this study. The lattice mismatches of the alloys were determined by the convergent beam electron diffraction technique (CBED) which was carried out on a transmission electron microscope (Philips CM30) at 100 kV. This microscope is fitted with a 'super Twin' lens and a double-tilt holder which could be turned by 30°. CBED patterns are obtained by tilting the phase of interest to the desired zone axis (a [1 1 4] zone axis was used in the present study). A computer program [25], involving a kinematical calculation was used so that the HOLZ lines in the central discs of the various CBED patterns could be simulated. Pure Si with its known lattice parameter (0.5429 nm) was used as a standard. The unknown electron wavelength was determined by varying this parameter in the computer simulation until the best match with the experimental CBED pattern of Si was established. Thin foils for CBED investigation were prepared as follows. First, a slice (2.3 mm in diameter, 0.8 mm thick) with faces parallel to [100] was cut from a sample by spark erosion. The slice was then mechanically thinned to a thickness of about 0.2 mm. Afterwards, the slice was dimpled and electropolished in a nitric acid/methanol solution (20% $HNO_3$ by volume) by using a twin-jet apparatus at 213 K. The electropolishing was performed at a voltage of 10 V and at a current of 10 mA. A 100 μm condenser (C2) aperture and a 3.5 nm spot size were used in the present work. In order to avoid temperature effects the samples were cooled by a cold stage with liquid nitrogen.

Both alloys were solution treated at 1473 K (alloy A) and 1573 K (alloy B) for 24 h, cooled down to an ageing temperature of 1413 K (alloy A) or 1443 K (alloy B), aged for durations ranging from 3–240 min (alloy A) and from 10–180 min (alloy B), and finally quenched into iced water. After etching (1% HF, 33% $HNO_3$, 33% $CH_3COOH$, 33% $H_2O$) scanning electron microscopy (SEM) was used to image the microstructure. Enlarged images were quantitatively analysed with an image analyser.

## 3. Results

The coarsening kinetics of the $\gamma'$ precipitates was studied in alloy A (Ni–13.5 at % Al) and alloy B (Ni–13.8 at % Al–5.9 at % Mo). The alloy A was aged at 1413 K and alloy B was aged at 1443 K. The average volume fractions of the precipitates ($f_v$) for both alloys at their ageing temperature are all about 20%.

The lattice mismatches for both alloys were measured by analysing around six CBED patterns recorded from different areas of the samples at room temperature. Fig. 1 shows a pair of representative experimental CBED patterns taken from alloy A after ageing at 1413 K for 120 min. This pattern gives the average value of the lattice mismatch calculated from six pairs of the CBED patterns. The corresponding

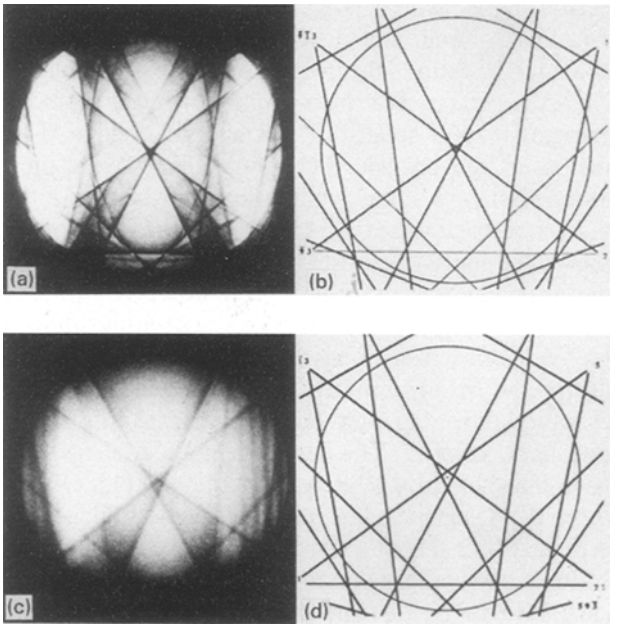


*Figure 1* Experimental and analytical HOLZ line patterns from the [114] zone axis for alloy A aged at 1413 K for 120 min. The experimental HOLZ line patterns are (a) from $\gamma'$, (c) from the $\gamma$ near the $\gamma'$. (b) and (d) show the corresponding computer similations. The lattice parameter of each phase is: $a_{\gamma'} = 0.3585$ nm, $a_{\gamma} = 0.3570$ nm. The lattice mismatch for this pair is 0.42%.

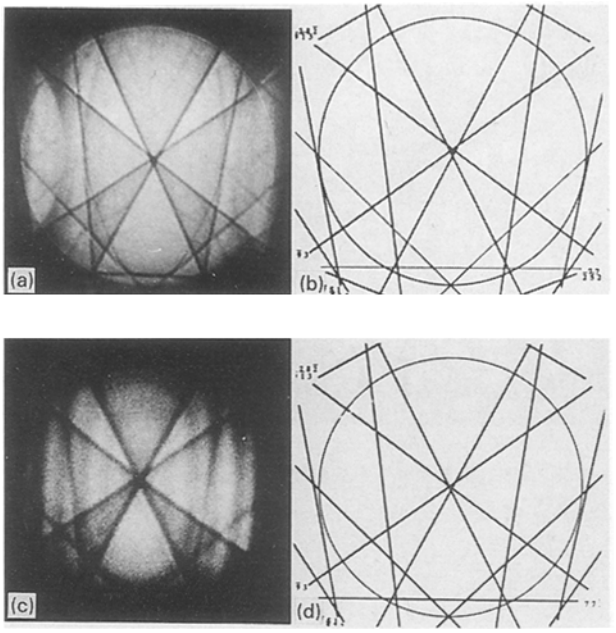


*Figure 2* Experimental and analytical HOLZ line patterns from the [114] zone axis for alloy B aged at 1443 K for 10 min. The experimental HOLZ line patterns are (a) from $\gamma'$, (c) from the nearby $\gamma$. (b) and (d) show the corresponding computer similations. The lattice parameter of each phase is: $a_{\gamma'} = 0.3588$ nm, $a_{\gamma} = 0.3593$ nm, $b_{\gamma} = 0.3590$ nm, $c_{\gamma} = 0.3593$ nm. The lattice mismatch for this pair is $-0.14\%$.

computer simulations are also shown in this figure. It has been observed that, as the ageing time increases, the change of the lattice parameter for precipitates and matrix is negligible [26]. By matching the experimental CBED patterns with the computer simulated patterns, a lattice mismatch of $\sim 0.42\,\%$ for alloy A at room temperature was obtained. By adjusting this value to incorporate the thermal expansion of $\gamma'$ and $\gamma$ ($\alpha_{\gamma'} = 1.32 \times 10^{-5}$ per °C, $\alpha_{\gamma} = 1.48 \times 10^{-5}$ per °C) [24] from room temperature to 1413 K, a positive mismatch of $\sim 0.25\,\%$ was obtained at 1413 K.

Fig. 2 shows a pair of representative CBED patterns (Fig. 2(a and c)) and the corresponding computer simulations (Fig. 2(b and d)) for alloy B. The lattice parameter of $\gamma'$ was about 0.3588 nm obtained by comparing the [114] CBED pattern (Fig. 2a) with the computer simulated pattern (Fig. 2b). The CBED pattern for the $\gamma$ matrix is not quite symmetric owing to the elastic strain (Fig. 2c). It was considered that the lattice parameter of the matrix in the "*b*" direction was reduced because of the smaller lattice parameter of the precipitates near the coherent $\gamma'/\gamma$ interface. The lattice parameters of the matrix in the "*a*" and the "*c*" directions were approximately equal to the unconstrained lattice parameter of the matrix, which is 0.3593 nm. The average lattice mismatch of alloy B is about $-0.14\%$ at room temperature. This value was obtained after alloy B had been aged for 10 min at 1443 K. By adjusting the values to incorporate the thermal expansion as stated above from room temperature to 1443 K, a larger negative mismatch of $-0.33\%$ can be estimated at 1443 K for alloy B.

Fig. 3 shows the morphological development of the $\gamma'$ particles with the ageing time for alloy A. Only the larger $\gamma'$ precipitates will be discussed here, since they were formed during the ageing, whilst the smaller precipitates were formed accidentally during the final quenching. The particles show cuboidal shape and are randomly distributed in the matrix during the early ageing times (Fig. 3(a– c)). A few particles show a tendency to split into doublets (Fig. 3c), and these splitting particles have apparently larger sizes (about 1312 nm) than the others (around 425 nm). After further ageing, the particles align along the ⟨100⟩ direction, form groups, and become inhomogeneously distributed (Fig. 3(d–f)). Fig. 4 shows the morphological changes of the $\gamma'$ particles with ageing time for alloy B. Some particles have split into two or four smaller ones after a relatively short ageing time (Fig. 4a). Fig. 4b shows the splitting particles with bigger magnification. After further ageing, the particles also align along the ⟨100⟩ direction and form groups, as observed for alloy A. Fig. 4f shows the morphology of the incoherent particles after 180 min of ageing. The particles contact each other and form rafts along ⟨100⟩. The above experimental observations show that the coarsening behaviours in the two alloys differ only at the early ageing stages, and that, after prolonged ageing, the morphological changes of the $\gamma'$ precipitates are very similar, i.e., the particles agglomerate and form groups.

The shape evolutions of the precipitates with ageing time has been estimated statistically by measuring about 1000 individual precipitates. The results are shown in Fig. 5 for alloy A and in Fig. 6 for alloy B. $K$ is the aspect ratio of the longest edge length to the shortest edge length of the cuboidal precipitates. The longest edge length was calculated through the value of the cross-sectional area of the particles along a ⟨100⟩ direction and the value of the shortest edge length, both of which can be measured by the image analysing program. Fig. 5a and Fig. 6a are the result of direct measurement from two-dimensional SEM views. On the other hand, Fig. 5b and Fig. 6b are obtained by assuming an equal distribution of the particle axis in three equivalent orientations, i.e., for $K \neq 1$, the number of distinct elongated particles counted in two-dimensional SEM views is actually only 2/3 of the total number of the particles. The other 1/3 of the total number of the particles with $K \neq 1$ were counted as particles with $K = 1$. It is observed that the tendency for precipitate shape change is similar for both alloys, but that the rates of change of the precipitate shape are different. For alloy A, particles with aspect ratio $K = 1$ represent the majority of all the particles up to nearly 100 min of ageing, but, for alloy B this period lasts only 30 min.

Figs 7 and 8 show histograms of the precipitate size distributions together with the plots from the LSW and the LSEM models. For both alloy A and alloy B, the PSDs are not independent of time, in contrast to theoretical prediction. The PSDs are symmetric and sharp during the early ageing times, but they become broader after prolonged ageing.

The precipitate size was obtained by regarding all shapes as a sphere of radius $R$. Fig. 9 presents two plots of the cube of the average radii of the precipitates

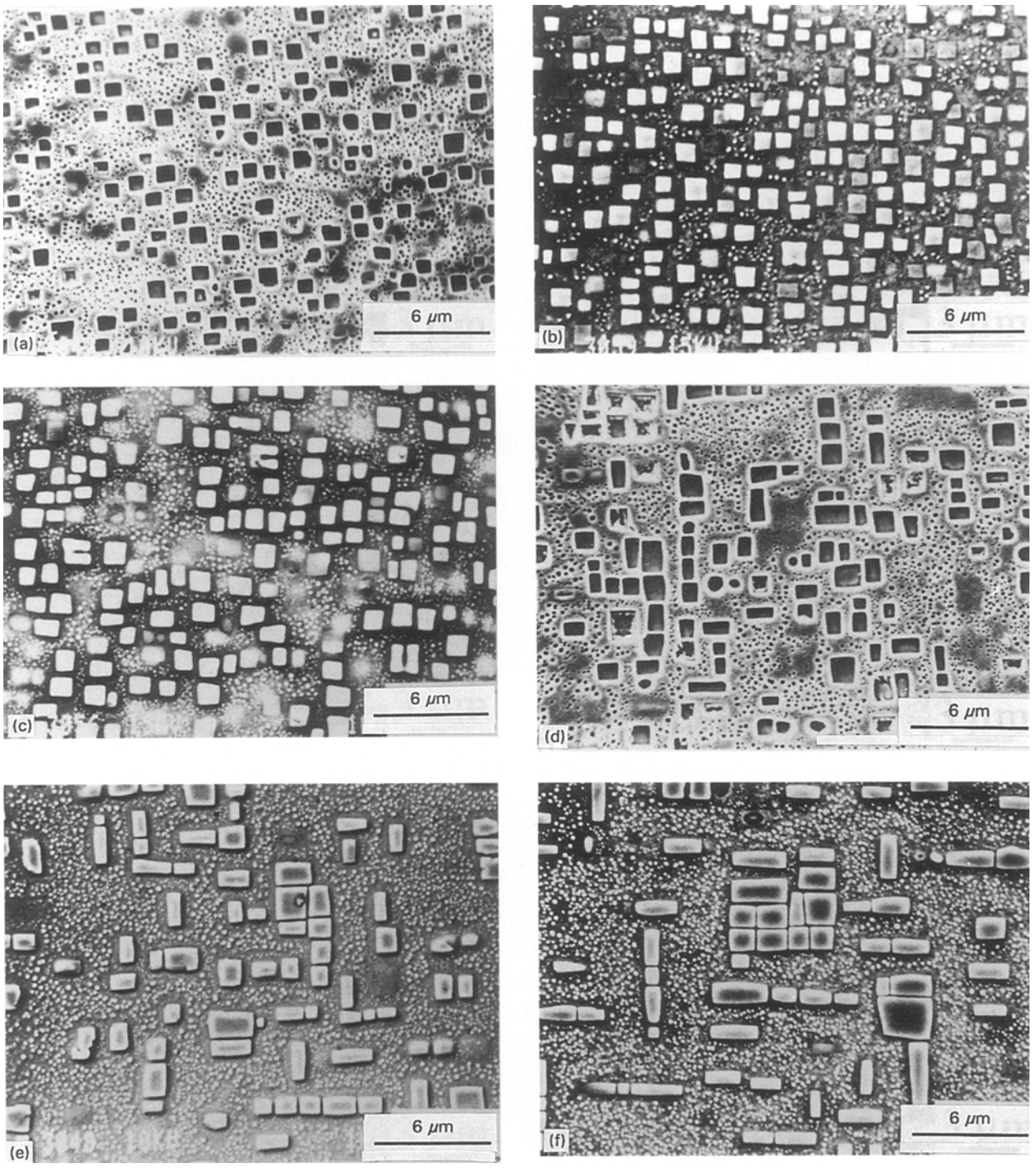


*Figure 3* The morphological development of γ′ particles (larger ones) for alloy A at 1413 K with the ageing time. (a) 3 min; (b) 6 min; (c) 12 min; (d) 60 min; (e) 120 min; (f) 240 min.

versus ageing time for alloy A (Fig. 9a) and for alloy B (Fig. 9b). None of the plots are linear, which is in contrast to the LSW theory. The average radii versus the ageing time in a log–log plot are shown in Fig. 10. The slope of the "best fit" line is $0.118 \pm 0.007$ for alloy A, and is $0.129 \pm 0.007$ for alloy B.

## 4. Discussion

The morphology, the size, and the size distribution of the particles were measured to determine the coarsening kinetics, and it was found that the kinetics for both alloy A and B were very different from the theoretical predictions [12–16]. The cube of the average size of the particles for both alloys was not found to be a linear function of the ageing time, as would be required for the LSW theory [12, 13] to hold. The growth rate of the particles varied with ageing time according to a power law with an exponent of $0.129 \pm 0.004$ for alloy A and $0.118 \pm 0.007$ for alloy B which are less than the 0.33 predicted by the LSW theory. This directly indicates that the elastic field produced by the lattice mismatch between the coherent precipitates and the matrix has a strong influence on the coarsening kinetics. Since alloy A and alloy B have nearly the same amount of the volume fraction

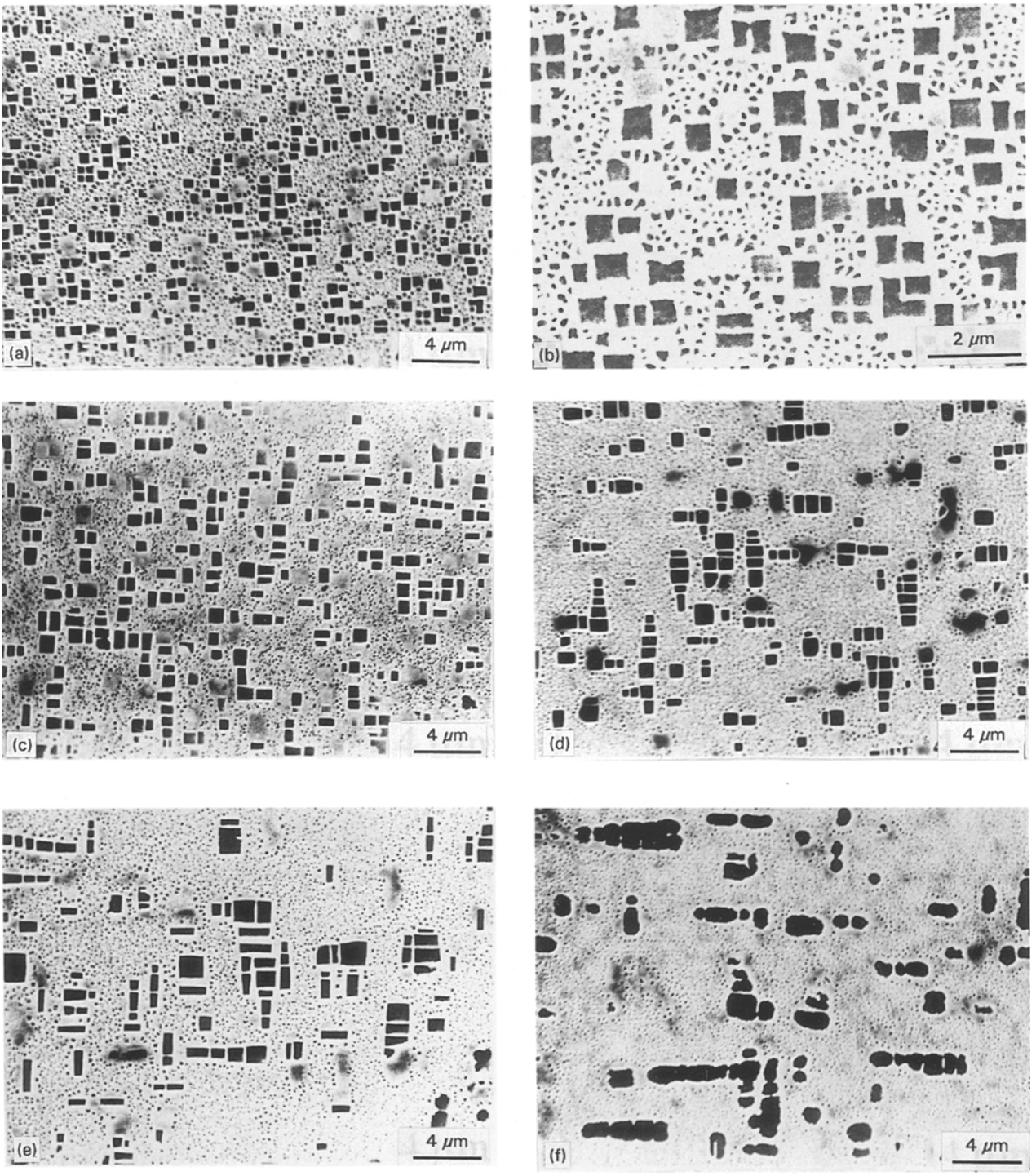


*Figure 4* The morphological development of γ′ particles (larger ones) for alloy B at 1443 K with the ageing time. (a) 10 min; (b) 10 min; (c) 40 min; (d) 74 min; (e) 120 min; (f) 180 min.

of precipitates, the slightly larger exponent for alloy A may be due to the smaller absolute value of the lattice mismatch (0.25%). Hein [10] also reported smaller time exponents (0.18, 0.25) for the growth rate in Ni–Al–Ti, which qualitatively agrees with our observation. A decreased exponent of the growth rate equation is also reported for various alloys [6, 9]. Enomoto and Kawasaki [19] indicated that the exponent of the growth law changes from 0.33 (predicted by LSW theory) to a smaller value for the alloy having negative mismatch and to a larger value (0.5) for positive mismatch after extensive ageing. However, the present experimental results show that the exponent of the growth law is reduced for the alloys with either positive or negative lattice mismatches.

At the early ageing time, the evaluation of the precipitates morphology is different between both alloys. For the Ni–Al alloy (alloy A) aged at 1413 K, neither doublets nor octets were observed. Only a few particles showed splitting leading to doublet formation and only after relatively long ageing times (Fig. 3). Most particles remained in cuboidal shape until the particles aligned and agglomerated into groups. This splitting behaviour is similar to the observation by

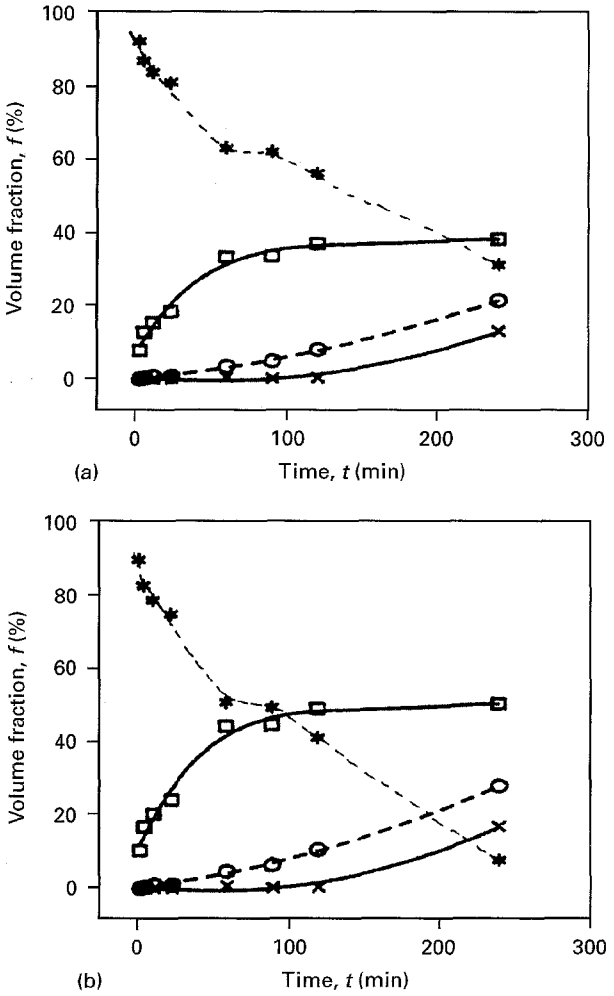


*Figure 5* The evolution of precipitate shape with ageing at 1413 K for alloy A. $K$ is the aspect ratio of the longest edge length and the shortest edge length of precipitates. (*) $K = 1$ means square; (□) $K = 2$ means rectangle; (○) $K = 3$ or (×) $K = 4$ means plate. (a) Direct measurement from two dimensional SEM pictures. (b) Three dimensional results by assuming an isotropic distribution of orientation of particles in three dimensions.

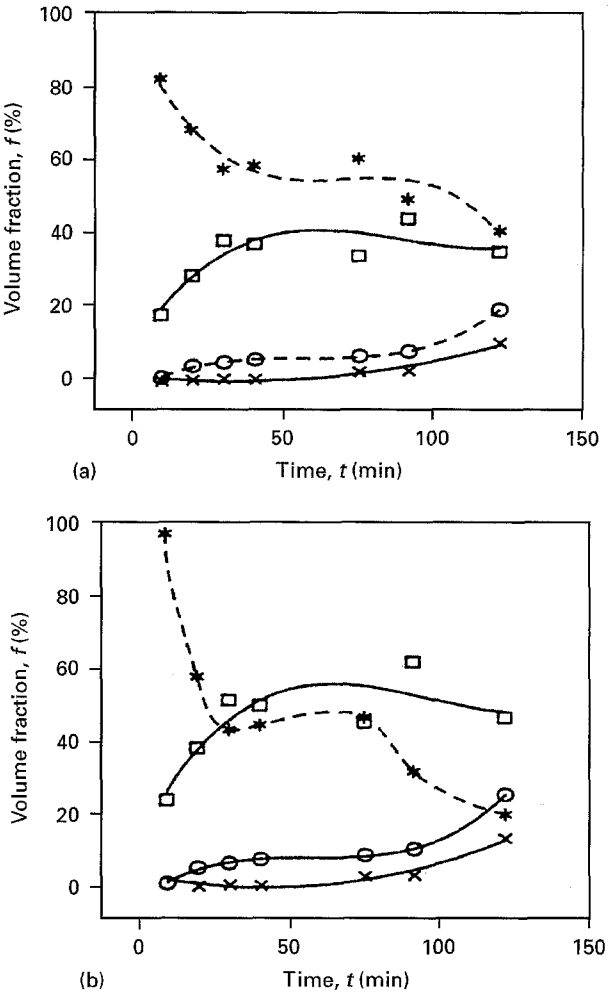


*Figure 6* The evolution of precipitate shape with ageing at 1443 K for alloy B. $K$ is the aspect ratio of the longest edge and the shortest edge of precipitates. (*) $K = 1$ means square; (□) $K = 2$ means rectangle; (○) $K = 3$ or (×) $K = 4$ means plate. (a) Direct measurement from two dimensional SEM pictures. (b) Three dimensional results by assuming an isotropic distribution of orientation of particles in three dimensions.

Miyazaki *et al.* [5]. They reported the doublet formation in Ni–12.0 at % Al aged at 1133 K for 20 h. Doi *et al.* [7] found that the $\gamma'$ particles in Ni–Al split into octets during slow cooling (0.1–0.01 K $s^{-1}$) from the solution temperature to the ageing temperature but that, for fast cooling (10–100 K $s^{-1}$), the particles do not split during the cooling at all. They can split into doublets during the ageing if the ageing temperature is just below the $\gamma'$ solvus line and the ageing is done for a long time (40 h). They explained the dependence of the splitting modes on the cooling rate in terms of whether there is enough time for the particles to grow and to exceed the critical size for the splitting to occur. We used a cooling rate of ~0.3 K $s^{-1}$ and this is larger than the slow cooling rate range but much smaller than the fast cooling rate range of Doi *et al.* [7].

In contrast to the Ni–Al system, the Ni–Al–Mo alloys had negative values for the mismatch. By using the same cooling rate, both doublets and octets were found after ageing the Ni–Al–Mo alloy for 10 min. The average edge length of the splitting particles in Ni–Al alloy is about 1312 nm. The average edge length of the doublets in Ni–Al–Mo is about 667 nm and is about 889 nm for the octet. Clearly, the critical sizes for particle splitting in the Ni–Al–Mo alloy are smaller than in the Ni–Al alloy. Therefore, the lattice mismatch can also influence the splitting behaviour through changing the critical sizes required for particle splitting.

Before the particles aligned and agglomerated into groups, the particles with an aspect ratio of $K = 1$ were dominant. Afterwards, particles with an aspect ratio of $K = 2$ became predominant and the particle shapes became nearly stable with longer ageing times. Such morphology evolutions of $\gamma'$ precipitates have not been documented up to date, although particle splitting [5, 7, 8], particle alignment [2], and inhomogeneous particle distribution [9] have been reported individually for the Ni–Al system. The present experiment found that, at early ageing times, particles split and produce a narrower size distribution. With increasing ageing time, particles agglomerate together and the size distribution of the particles becomes broader. These observations disagree with Miyazaki and Doi [6] who proposed that, in general, the size distribution of the particles should become narrower

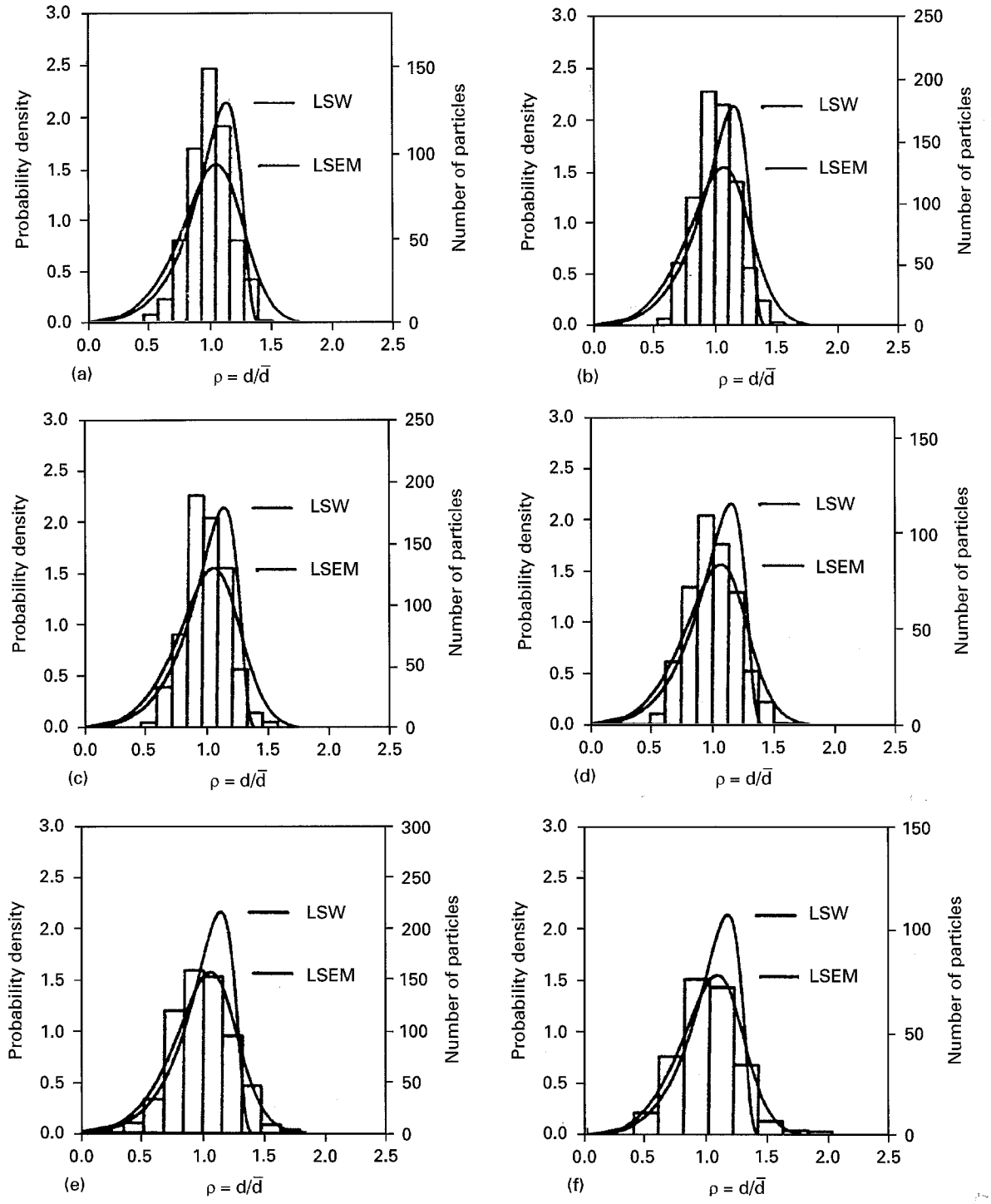


*Figure 7* The radius distribution of the precipitates for several ageing times at 1413 K for alloy A, (a) 3 min; (b) 6 min; (c) 12 min; (d) 24 min; (e) 90 min; (f) 240 min. The histograms represent the experimental results. Two solid lines represent the results predicted by the LSW [12, 13] and LSEM [15] theories, respectively.

with increasing ageing time in an elastically constrained system. Their observation was based on their study of the coarsening behaviours in Ni–Mo and Ni–Si and on their theoretical model based on bifurcation diagrams. However, the reason for these differences are not clear.

## 5. Conclusion

The coarsening kinetics of the $\gamma'$ precipitates as a function of the lattice mismatch without the influence of an external stress were investigated in single crystal Ni–Al(13.5 at %) and Ni–Al(13.8 at %)–Mo(5.9 at %). For the Ni–Al–Mo alloy having a lattice mismatch of about $-0.3\%$ at the ageing temperature, the precipitates were initially cuboidal and then they split mostly into two parallel plates (doublet) or eight sub-cubes (octet) after ageing for 10 min. After prolonged ageing, the precipitates eventually aligned and agglomerated into groups consisting of many particles separated by a small distance of $\sim 30$ nm, and the distribution of the precipitates became inhomogeneous. For the

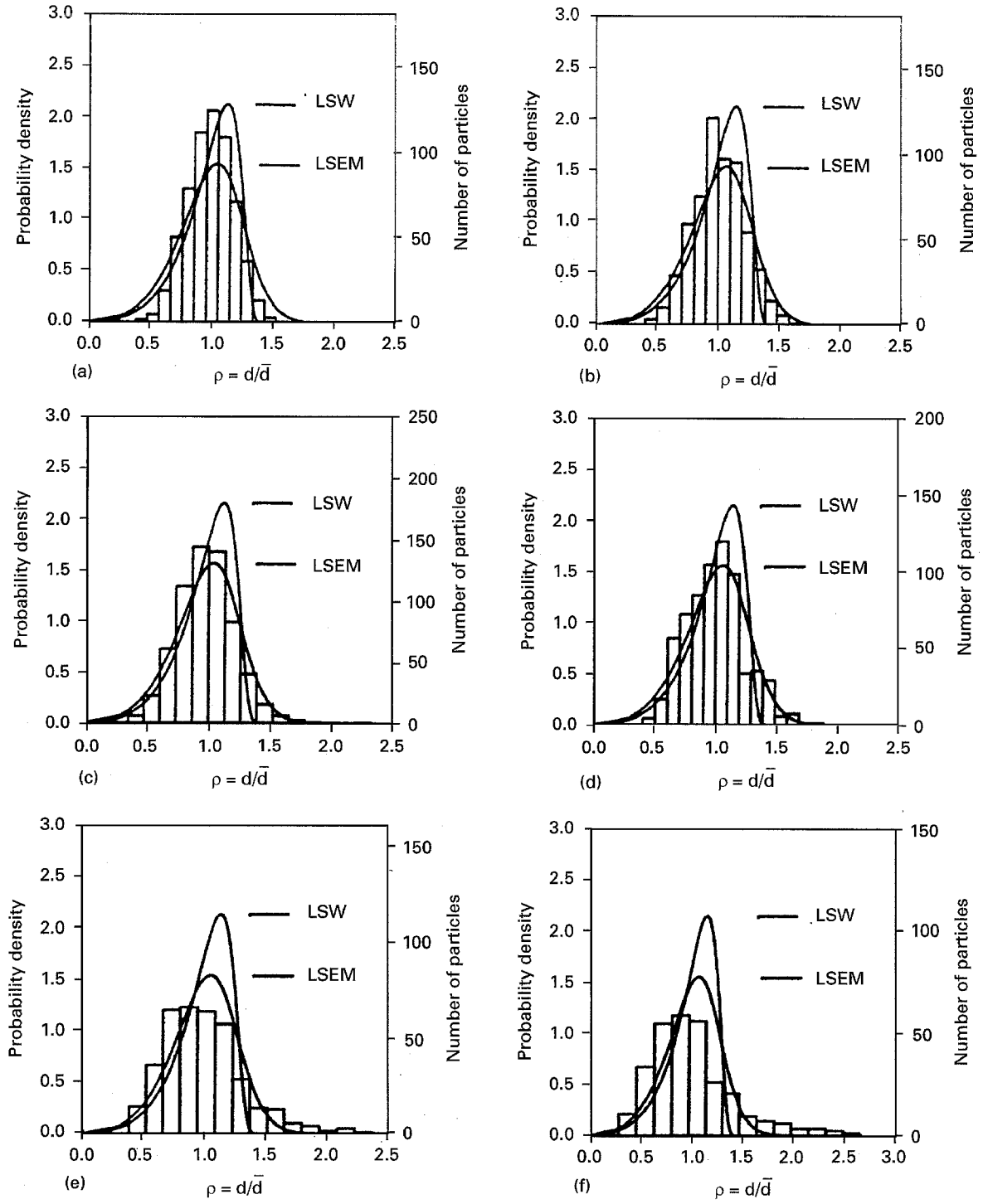


*Figure 8* The radius distribution of the precipitates for several ageing times at 1443 K for alloy B, (a) 10 min; (b) 20 min; (c) 40 min; (d) 90 min; (e) 120 min; (f) 180 min. The histograms represent the experimental results. Two solid lines represent the results predicted by the LSW [12, 13] and LSEM [15] theories, respectively.

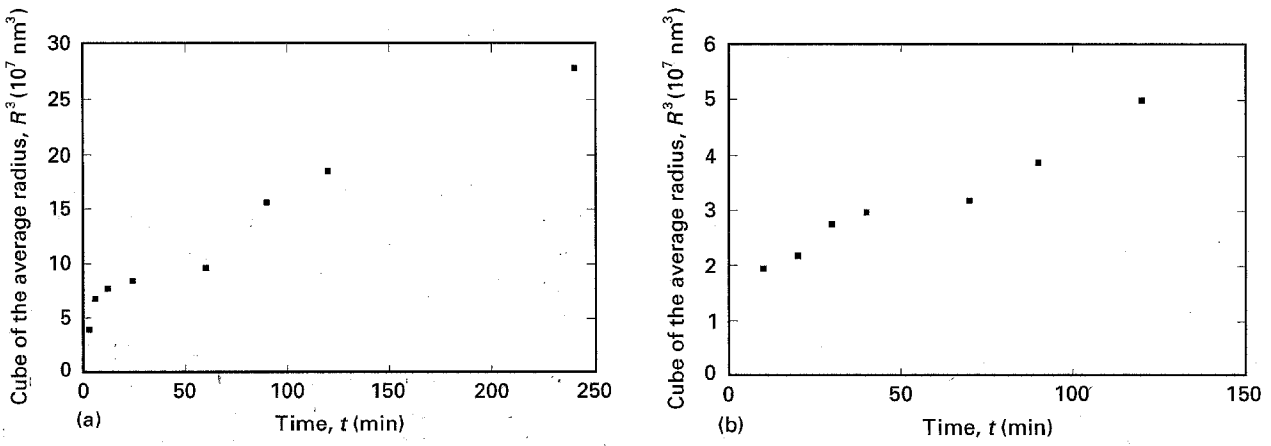


*Figure 9* Changes of the cube of the average radius $R$ of the precipitates with ageing time, (a) for alloy A at 1413 K, (b) for alloy B at 1443 K.

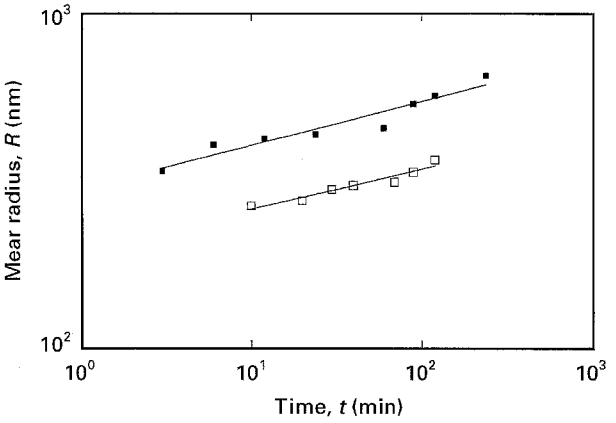


*Figure 10* Mean radius $R$ of the precipitates as a function of ageing time $t$ in a log–log representation for, (■) alloy A and (□) alloy B. For alloy A, $R = 301.56 \times t^{0.12931}$, for alloy B, $R = 200.26 \times t^{0.11822}$.

Ni–Al alloy having a positive mismatch, the original cuboidal particles only showed the tendency to split into doublets. After a longer ageing time, the development of the morphology of the $\gamma'$ precipitates was the same as that found in the Ni–Al–Mo alloys, i.e. the particles aligned and formed groups. The evolution of the precipitates shape during the ageing process was measured and analysed statistically by assuming an isotropic distribution of the precipitate orientation in three dimensions. The result showed that: (1) at the beginning of the ageing, most of the precipitates had a cuboidal shape with an aspect ratio $K \sim 1$, and (2) after the precipitates formed groups, most of the precipitates elongated to have an aspect ratio $K \sim 2$. Furthermore, the size distribution of the precipitates became broader with increasing ageing time. There was no linear relationship between the cube of the average precipitate size and the ageing time as predicted by the classical Lifshitz–Slyozov–Wagner (LSW) theory.

## References


1. J. CONLEY, M. E. FINE and J. R. WEERTMAN, *Acta. Metall. Mater.* **37** (1989) 1251.
2. A. J. ARDELL, R. B. NICHOLSON and J. D. ESHELBY, *Acta. Metall. Mater.* **14** (1966) 1295.
3. S. J. YEOM, D. Y. YOON and M. F. HENRY, *Metall. Trans.* **24A** (1993) 1975.
4. A. D. SEQUEIRA, H. A. CALDERON and G. KOSTORZ, *Scripta Metall.* **30** (1994) 7.
5. T. MIYAZAKI, H. IMAMURA, T. KOZAKAI, *Mater. Sci. Engng.* **54** (1982) 9.
6. T. MIYAZAKI and M. DOI, *Ibid.* **A110** (1989) 175.
7. M. DOI, T. MIYAZAKI and T. WAKATSUKI, *Ibid* **74** (1985) 139.
8. M. J. KAUFMAN, P. W. VOORHEES, W. C. JOHNSON and F. S. BIANCANIELLO, *Metall. Trans.* **A20** (1989) 2171.
9. T. MIYAZAKI, M. DOI and T. KOZAKI, *Solid St. Phen.* **3&4** (1988) 227.
10. H. HEIN, *Acta Metall. Mater.* **37** (1989) 2145.
11. Y. Y. QU, H. A. CALDERON and G. KORSTORZ, In "Solid–Solid Phase Transformations" (PTM '94), edited by W. C. Johnson, J. M. Howe, D. E. Laughlin and W. A. Soffa (The Minerals, Metals and Materials Society, 1994) pp. 509–604.
12. I. M. LIFSHITZ and V. V. SLYOZOV, *Phys. Chem. Solids* **11** (1961) 35.
13. C. WAGNER, *Z. Electrochem.* **65** (1961) 581.
14. A. D. BRAILSFORD and P. WYNBLATT, *Acta Metall. Mater.* **27** (1979) 489.
15. C. K. L. DAVIES, P. NASH and R. N. STEVENS, *Ibid.* **28** (1980) 179.
16. M. TOKUYAMA and M. KAWASAKI, *Physica* **123A** (1984) 386.
17. A. G. KHACHATURYAN, S. V. SEMENOVSKAYA and J. W. MORRIS, *Acta Metall. Mater.* **36** (1988) 1563.
18. H. NISHIMORI and A. ONUKI, *Phys. Rev. B* **42** (1990) 980.
19. Y. ENOMOTO and K. KAWASAKI, *Acta Metall.* **41** (1993) 279.
20. R. C. ECOB, M. P. SHAW, A. J. PORTER and B. RALPH, *Phil. Mag.* **A44** (1981) 1117.
21. R. C. ECOB, R. A. RICKS and A. J. PORTER, *Scripta Metall.* **16** (1982) 1085.
22. M. J. KAUFMAN, D. D. PEARSON and H. L. FRASER, *Phil. Mag.* **A54** (1986) 79.
23. A. J. PORTER, R. C. ECOB and R. A. RICKS, *J. Microsc.* **129** (1983) 327.
24. H. L. FRASER, D. M. MAHER, C. J. HUMPHREYS, C. J. D. HETHERINGTON, R. B. KNOELL and J. C. BEAN, *Inst. Phys. Conf. Ser.* **76** (1985) 307.
25. P. STADELMANN, Unpublished results. 1993, 12M-EPFL, Switzerland.
26. YANYAN QIU, Ph.D thesis. ETH-Zurich. (1994)



*Received 5 July 1995*
*and accepted 21 December 1995*